# Chapter 7

# Effect of Impurity Doping at the Schottky Interface

## 7.1 Introduction

Schottky barriers can be strongly modified by presence of impurities at the interface. Typical examples are the occurrence of unintended interface states, deep level trap states in semiconductors and secondary phase formation at the interface [1]. Due to the large difference in the bonding nature of elemental metal and covalent semiconductors, the interface structure tends to be amorphous or polycrystalline, and the effect of impurities results as modification in the electronic structure of the *semiconductor* side with small influence on the metal side.

Compared with a conventional Schottky junction, a perovskite oxide Schottky junction is expected to show significant differences on the effect of impurities at the *metal* side of the interface.

Perovskite Schottky junctions are composed of elements of similar characteristics, namely the B-site cations are transition metal ions on both sides, which makes the interface chemical bonds less dissimilar than conventional Schottky junctions. This is mainly due to the fact that the conductivity in perovskite oxides arise from the subtle energy balance between different competing interactions, and not from the fundamental difference in the electronic configuration [2]. If impurities are introduced to such interfaces, two interesting effects can be anticipated.

First, depending on the type of impurity, the electronic structure in the metal will be strongly modified, possibly undergoing a insulator to metal transition as seen often in bulk [2]. The close chemical characteristics and the small lattice mismatch easily allow formation of epitaxial interfaces, resulting in one part of the interface being strained. Therefore, the bulk prediction of a drastic phase transition is not always present at interfaces [3]. The second effect is the formation of localized states on the *metal* side. The bandwidth of perovskite oxide metals are generally much narrower than that of elemental metals, due to the more localized nature of the $d$-orbitals. If the wave function of the impurity atoms have insufficient overlaps with the host wave functions, these may form independent states. The effect of such localized state formation at the interface would lead to a method for designing new

functionalities within a simple structure.

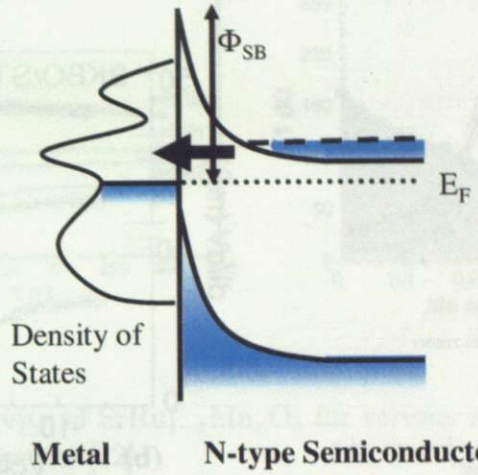


Figure 7.1: Illustration of the application of Schottky junctions for tunneling spectroscopy, probing the density of states on the metal side using the inherent depletion width as the tunnel barrier.

In order to characterize the interface electronic structure in Schottky junctions, tunneling spectroscopy is an ideal technique [4], for its high sensitivity to the electronic structures on the scale of $< 1$ eV(Fig. 7.1). Studies in the special case of superconductor-semiconductor Schottky junctions has been reported as shown in Fig. 7.2 for Pb/GaAs ((a)) and $Ba_{1-x}K_xBiO_3$/Nb:$SrTiO_3$ ((b)). Here the depletion region, which is tunable by the doping concentration in the semiconductor, is used as the barrier layer in the tunneling structure.

For the purpose of studying the effect of the presence of impurities at the interface, a junction between Mn-doped $SrRuO_3$ and Nb:$SrTiO_3$ is studied as a model system.

$SrRuO_3$ is a highly conducting metal in the absence of chemical substitution, and its physical properties are governed by the $4d$ character of Ru, which is spatially more distributed to hybridize with oxygen ions compared with the $3d$ transition metal ions. The physical properties of $SrRuO_3$ are sensitive to disorder induced by chemical doping such as Ca [7], Pb [8], Zn, Ni, Co [9], Fe [10] or Mn [9, 11, 12], inducing a metal-insulator transition by doping. In the case of doping by a $3d$ transition metal ion at the Ru site, the hybridization of the Ru is reduced because of the localized nature of the $3d$ orbitals as seen in Mn-doped $CaRuO_3$ [13] and Mn doped $Sr_3Ru_2O_7$ [14]. Appearance of similar localized states can be expected for Mn-doped $SrRuO_3$, which if located at the interface could result in an interface state. The presence of impurity at the interface is also expected to cause more fluctuation in the barrier height due to the additional electrostatic potential, which would increase the spatial inhomogeneity of the SBH. Fig. 7.3 illustrates the two effects predicted to arise from Mn doping at Mn:$SrRuO_3$/Nb:$SrTiO_3$ Schottky junction.

The use of Nb:$SrTiO_3$ as the semiconductor has two features to be addressed. First is the wide spread use of Nb:$SrTiO_3$ as a standard semiconductor in perovskite

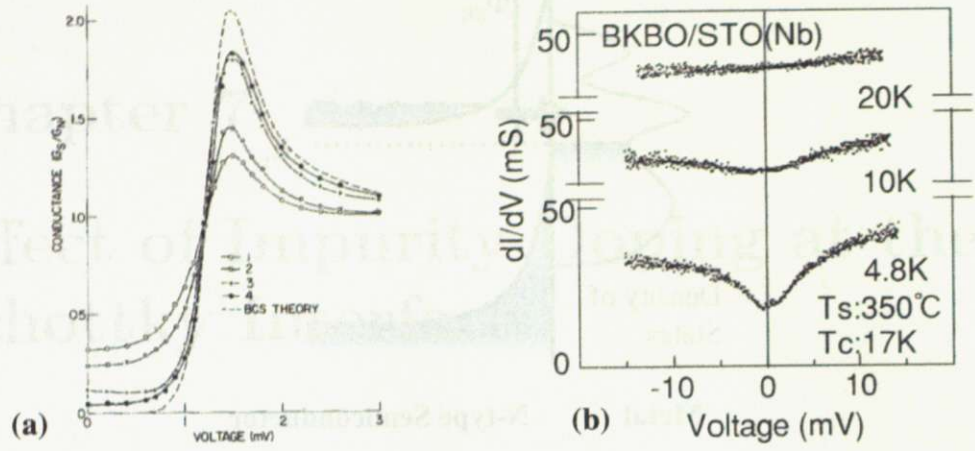


Figure 7.2: Tunneling conductance versus voltage for (a) Pb/$p$-GaAs at 1.34 K for different surface preparation [5], and (b) $Ba_{1-x}K_xBiO_3$/Nb:$SrTiO_3$ at different temperatures [6].

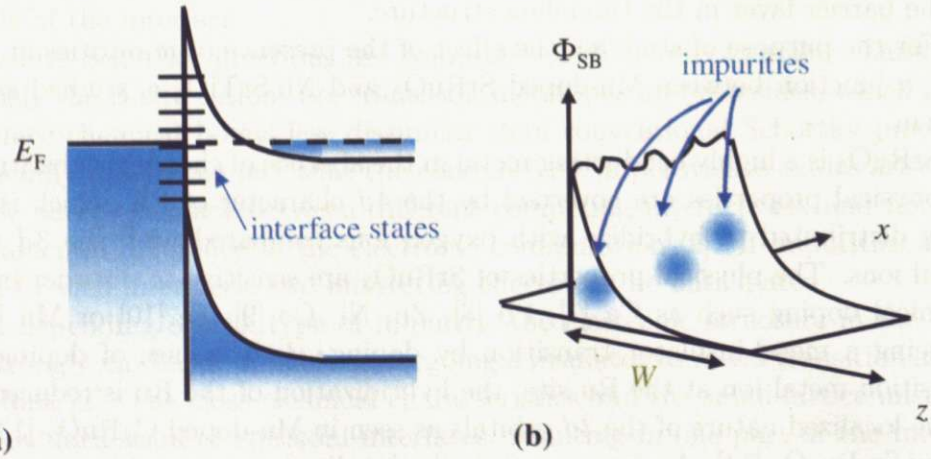


Figure 7.3: Illustration of the possible effects of impurities at the interface. (a) Formation of interface states and (b) increase in the spatial inhomogeneity in the barrier potential.

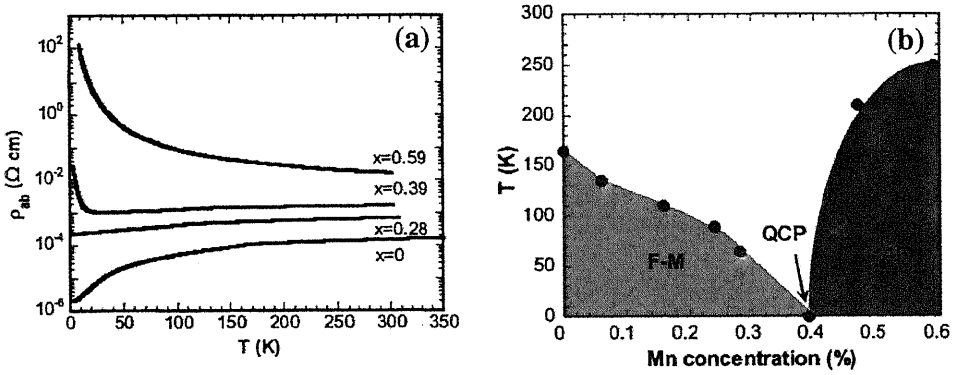


Figure 7.4: (a) Resistivity of $SrRu_{1-x}Mn_xO_3$ for various $x$ and the magnetic phase diagram of the same system [12].

oxide devices, and secondly its strong electric field dependent dielectric permittivity influencing the band bending as has been investigated in this thesis. The non-parabolic band bending in the semiconductor evident at low temperature results in steeper band bending and a narrower depletion region, which is an ideal situation where Nb:$SrTiO_3$ can be used as an effective emitter accommodating a variable barrier thickness in tunneling experiments.

## 7.2 Motivation

The motivation of this study is to investigate the effect of impurities at the interface in perovskite oxide Schottky junctions. Mn:$SrRuO_3$/Nb:$SrTiO_3$ is studied as a model system with reference to $SrRuO_3$/Nb:$SrTiO_3$. $I$-$V$ characteristics will be used to probe the effect of impurities on the electronic structure at the interface.

## 7.3 Band Bending Calculations

The investigation of $SrRuO_3$/Nb:$SrTiO_3$ Schottky junctions has demonstrated an exclusive feature of $SrTiO_3$ in which its dielectric permittivity is strongly modulated by electric field, varying the electrostatic potential at the interface. In order to grasp a quantitative understanding, we have performed simulations of various physical parameters relevant in Schottky junctions using the formulae from Yamamoto *et al.* [15] mentioned earlier. Eq. (5.8) is used for the electrostatic potential, Eq. (5.9) for the electric field and Eq. (5.4.4) for the dielectric permittivity. The donor concentration and the SBH have been used as the variable parameters.

Without the electric field dependence, the depletion width is expected to increase as the temperature is reduced because of the increase in $\epsilon_S$ according to Barrett's formula, as observed in Fig. 7.5(d). However, the strong electric field at the interface decreases $\epsilon_S$, reducing the depletion width with decrease in temperature

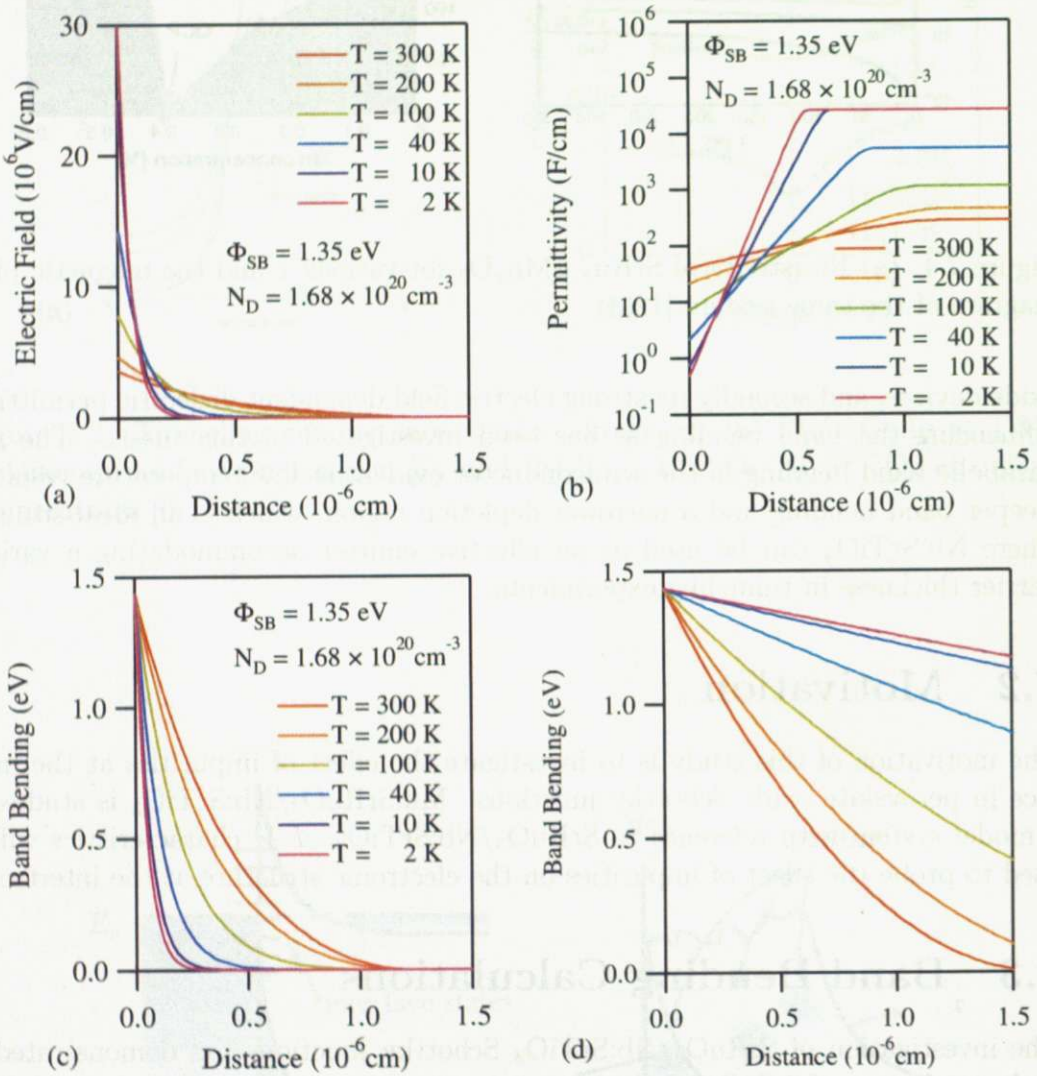


Figure 7.5: (a)Electric field, (b) dielectric permittivity, (c) electrostatic potential as a function of distance from the interface using Eq. (5.8), (5.9), (5.4.4). (d) Electrostatic potential calculated based on temperature dependence and no electric field dependence. $\Phi_{SB} = 1.35$, $N_D = 1.68 \times 10^{20}$ cm$^{-3}$.

(Fig. 7.5(c)). This behavior enables tuning of the band bending in heterostructures by changing the donor concentration, which is an exclusive degree of freedom to $SrTiO_3$ not available in a conventional semiconductor. These results show that $SrRuO_3$/Nb:$SrTiO_3$ under these doping conditions have sufficiently narrow depletion width for tunneling experiments.

## 7.4 Experimental

### 7.4.1 Optimization of the Growth Conditions

In order to fabricate Mn:$SrRuO_3$/Nb:$SrTiO_3$ Schottky junctions using PLD, basic characterization of the thin films was carried out by varying the following parameters in the growth of $SrRuO_3$/$SrTiO_3$(001):

1. laser fluency
2. substrate temperature
3. oxygen partial pressure.

The structural characterization was carried out using XRD and electrical transport characterization by resistivity measurements as a function of temperature. All films exhibited epitaxial growth from the absence of diffraction peaks other than $(00n)$. The measured XRD diffraction patterns and the resistivity results are shown in Figs. 7.6 and 7.7. These results indicate that out of the three growth parameters, the laser fluency and the oxygen partial pressure are the two dominant growth parameters. Increase in the laser fluency sharpens the XRD peak associated with the shrinking of the out-of-plane lattice constant and lowers the resistivity of the films. An increase in the oxygen partial pressure also decreases the out-of-plane lattice constant and reduces the resistivity of the films. The effect of substrate temperature has a smaller effect compared with the other two with similar tendencies to previous reports [16, 17].

### 7.4.2 Basic Characterization

Following the above results, the growth conditions for the investigation in $I$-$V$ characteristics in Mn:$SrRuO_3$/Nb:$SrTiO_3$ are summarized in Table 7.1 The XRD diffraction pattern and the temperature dependent resistivity of the fabricated thin films of Mn:$SrRuO_3$ and $SrRuO_3$ on $SrTiO_3$(001) are shown in Fig. 7.8. XRD revealed epitaxial growth and an out-of-plane lattice constant of 3.95 Åin both cases. The resistivity of the films exhibited a metallic behavior with a change in the slope at 140 K and 150 K corresponding to the ferromagnetic ordering temperature ($T_C$) for Mn:$SrRuO_3$ and $SrRuO_3$ respectively. The slight decrease in $T_C$ and the increased residual resistivity compared to undoped counterparts can be ascribed mainly to the effect of Mn doping.

For the $I$-$V$ measurements, the grown samples were cut into 0.3 mm $\times$ 0.3 mm squares and electrical contacts were made by Ag paste directly on Mn:$SrRuO_3$

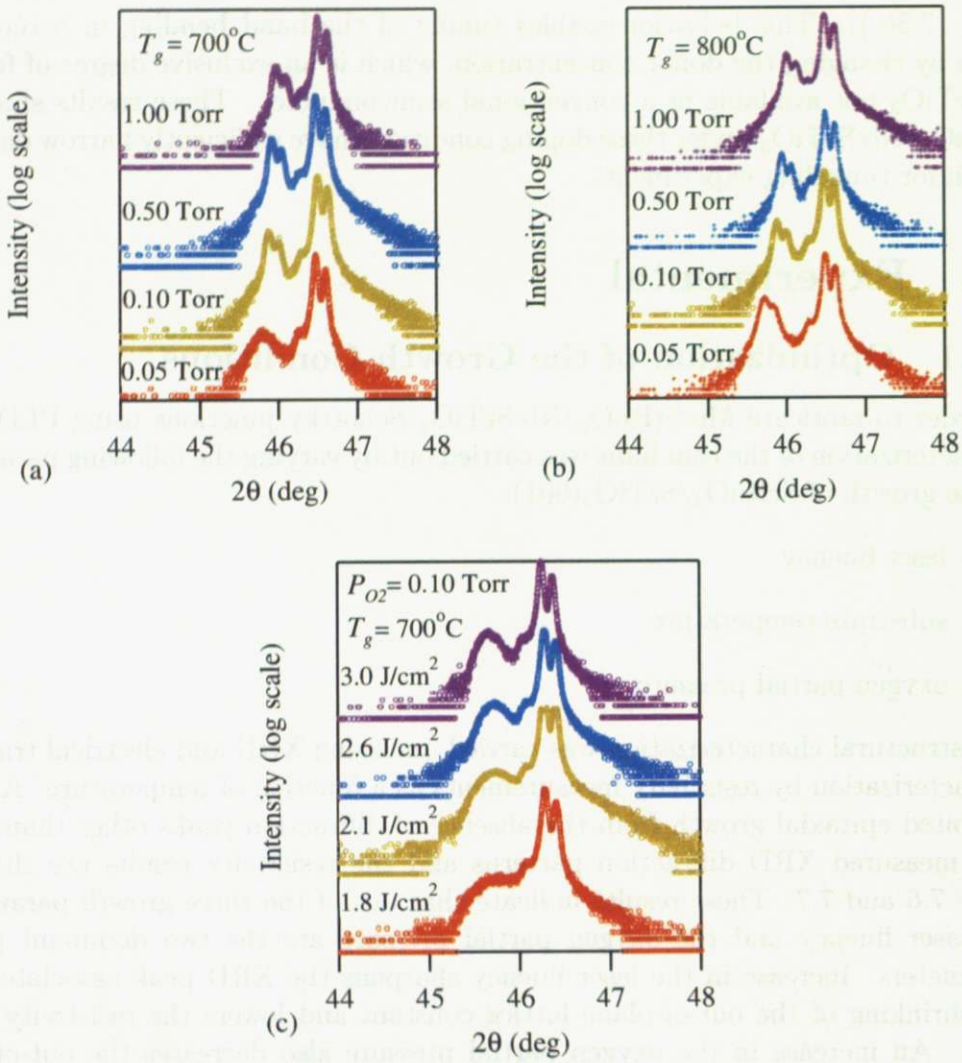


Figure 7.6: XRD pattern of $SrRuO_3/SrTiO_3$ (001) at various growth conditions. Varying pressure at constant laser fluency $F = 2.6$ J/cm$^2$ at substrate temperature of (a) $T_g = 700$°C, (b) $T_g = 800$°C, and (c) varying the laser fluency at constant $T_g = 700$°C and pressure, $P_{O2} = 0.1$ Torr.

Table 7.1: Growth conditions for the 5 mol% Mn doped $SrRuO_3/Nb{:}SrTiO_3$ Schottky junctions.

| | |
|---|---|
| Substrate | Nb:$SrTiO_3$ |
| | Nb = 0.5 wt % |
| Oxygen Partial Pressure (Torr) | 0.3 |
| Substrate Temperature (°C) | 800 |
| Laser Fluency (J/cm$^2$) | 2.0 |
| Laser Frequency | 8 Hz |
| Ablation Target | Polycrystalline $SrRuO_3$ |

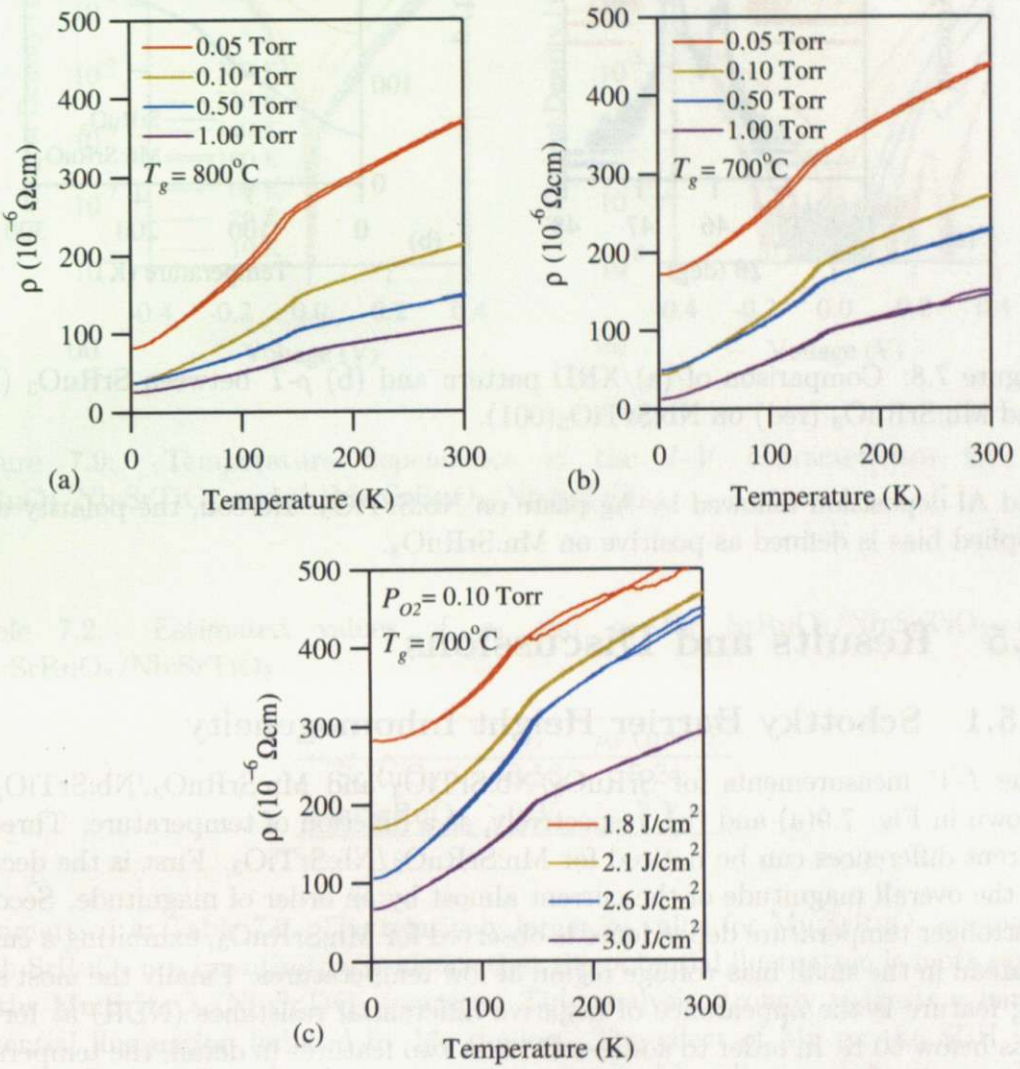


Figure 7.7: $\rho$-$T$ of $SrRuO_3/SrTiO_3$ (001) at various growth conditions. Varying pressure at constant laser fluency $F = 2.6$ J/cm$^2$ at substrate temperature of (a) $T_g = 700$°C, (b) $T_g = 800$°C, and (c) varying the laser fluency at constant $T_g = 700$°C and pressure, $P_{O2} = 0.1$ Torr.

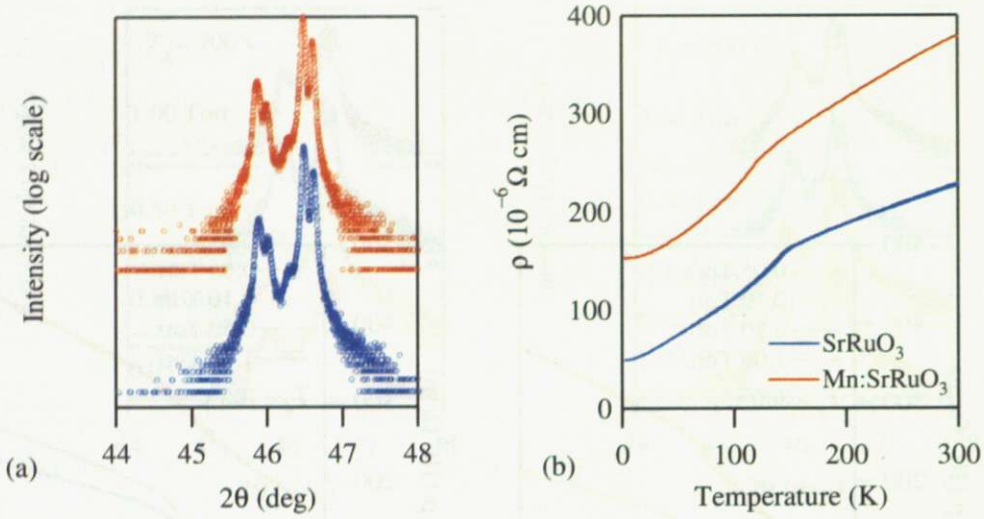


Figure 7.8: Comparison of (a) XRD pattern and (b) $\rho$-$T$ between $SrRuO_3$ (blue) and Mn:$SrRuO_3$ (red) on Nb:$SrTiO_3$(001).

and Al deposition followed by Ag paste on Nb:$SrTiO_3$. Hereon, the polarity of the applied bias is defined as positive on Mn:$SrRuO_3$.

## 7.5 Results and Discussions

### 7.5.1 Schottky Barrier Height Inhomogeneity

The $I$-$V$ measurements for $SrRuO_3$/Nb:$SrTiO_3$ and Mn:$SrRuO_3$/Nb:$SrTiO_3$ are shown in Fig. 7.9(a) and (b), respectively, as a function of temperature. Three apparent differences can be noticed for Mn:$SrRuO_3$/Nb:$SrTiO_3$. First is the decrease in the overall magnitude of the current almost by an order of magnitude. Secondly a stronger temperature dependence is observed for Mn:$SrRuO_3$, exhibiting a current plateau in the small bias voltage region at low temperatures. Finally the most striking feature is the appearance of negative differential resistance (NDR) at forward bias below 60 K. In order to address the first two features in detail, the temperature dependence of the ideality factor was analyzed following the discussion of the effect of spatial inhomogeneities on Schottky barrier heights [18].

A phenomenological parameter of the degree of inhomogeneity in Schottky junctions is the temperature dependence of the ideality factor. On the assumptions of a Gaussian distribution and a voltage dependence in the SBH give us the following relationship, which agrees well with many experimental results.

$$\frac{1}{n(T)} - 1 = -\rho_2 + \frac{\rho_3}{2kT/q} \tag{7.1}$$

Here, $\rho_2$ gives the degree of the SBH sensitivity to applied voltage and $\rho_3$ corresponds to the standard deviation in SBH. Eq. (7.1) tells us that a larger $\rho_3$ implies a Schottky junction with a larger distribution of SBH. The present results plotted

following Eq. (7.1) is shown in Fig. 7.10. The estimated values from Fig. 7.9 are

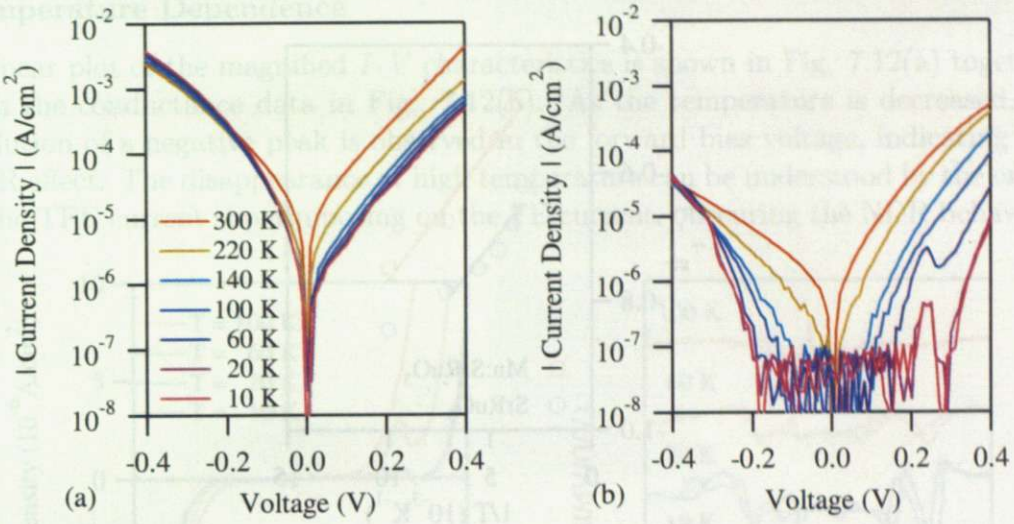


Figure 7.9: Temperature dependence of the $I$-$V$ characteristics for (a) $SrRuO_3$/Nb:$SrTiO_3$ and (b)Mn:$SrRuO_3$/Nb:$SrTiO_3$.

Table 7.2: Estimated values of $\rho_2$ and $\rho_3$ for $SrRuO_3$/Nb:$SrTiO_3$ and Mn:$SrRuO_3$/Nb:$SrTiO_3$.

| | $\rho_2$ | $\rho_3$ (meV) |
|---|---|---|
| $SrRuO_3$ | -0.56 | 5.24 |
| Mn:$SrRuO_3$ | -0.35 | 7.1 |

summarized in Table 7.2. The relatively larger $\rho_3$ value for Mn:$SrRuO_3$ compared with $SrRuO_3$ is a quantitative evidence that the potential fluctuation is more severe in the Mn:$SrRuO_3$/Nb:$SrTiO_3$ junction. This analysis strongly suggests a barrier potential fluctuation induced by Mn doping. The effect of Mn on the SBH may include effects such as local distribution in chemical bonding or dislocations. It is also possible that doped Mn ions have diffused to the Nb:$SrTiO_3$ depletion region creating trap states modifying the band bending in the semiconductor.

The current transport mechanism in these junctions can be determined from the plot of $J_S/T^2$ versus $1/T$ plot shown in Fig. 7.11(a). The saturation of $J_S/T^2$ at low temperatures is similar to what has been observed in Au/Nb:$SrTiO_3$ Schottky junctions [19] corresponding to the dominance of the field emission process. Therefore the low temperature current transport can be said to be of tunneling origin as we have expected. Since the NDR behavior is observed in this tunneling dominating temperature region, formation of a resonant state is suspected similar to the case of double barrier resonant tunneling diode [20].

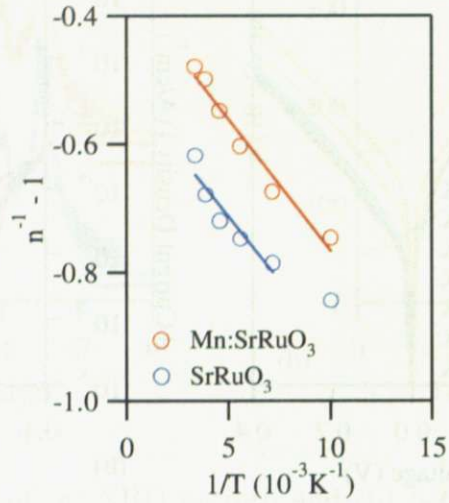


Figure 7.10: Evaluation of the Schottky barrier height spatial inhomogeneity from the ideality factors for $SrRuO_3$ /Nb:$SrTiO_3$ and Mn:$SrRuO_3$ / Nb:$SrTiO_3$.

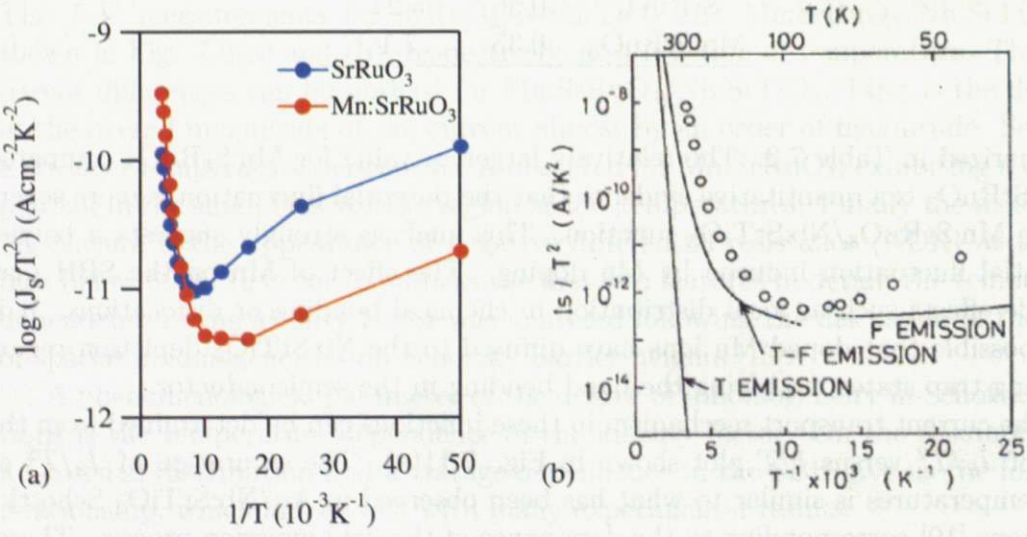


Figure 7.11: Richardson plot of (a) $SrRuO_3$/Nb:$SrTiO_3$ and Mn:$SrRuO_3$/Nb:$SrTiO_3$ junctions showing similar behavior to (b) Au/Nb:$SrTiO_3$ [19].

### 7.5.2 Tunneling Conductance

#### Temperature Dependence

A linear plot of the magnified $I$-$V$ characteristics is shown in Fig. 7.12(a) together with the conductance data in Fig. 7.12(b). As the temperature is decreased, an evolution of a negative peak is observed in the forward bias voltage, indicating the NDR effect. The disappearance at high temperature can be understood by the onset of the TFE current superimposing on the FE current, obscuring the NDR behavior.

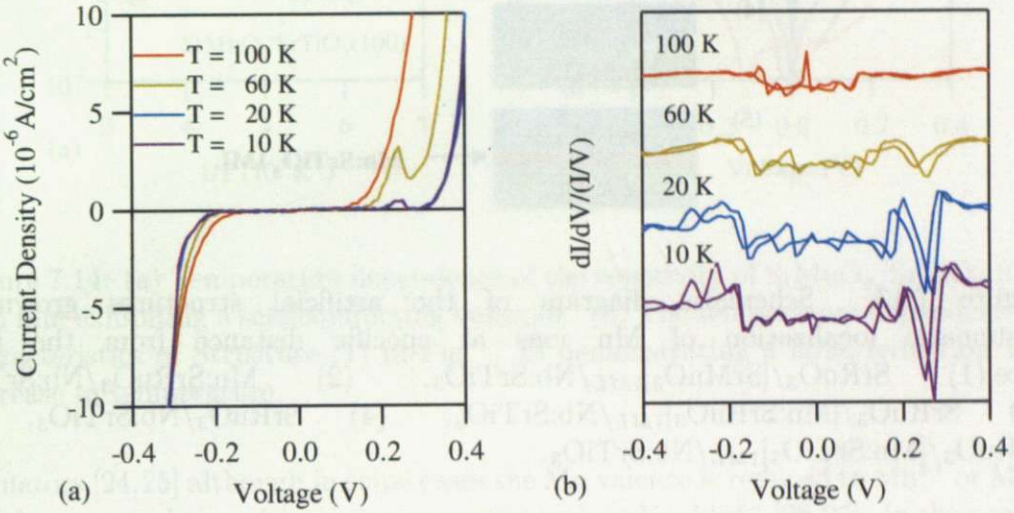


Figure 7.12: Temperature dependence of (a) the $I$-$V$ and (b) the normalized conductance of Mn:$SrRuO_3$/Nb:$SrTiO_3$ junction.

The observation of an NDR in Mn:$SrRuO_3$/Nb:$SrTiO_3$ has led us to investigate $I$-$V$ characteristics in other structures. The absence of the NDR behavior in $SrRuO_3$/Nb:$SrTiO_3$ strongly indicates that the presence of Mn ions is a requirement for the occurrence of this behavior.

#### Artificial Modulation of Interfaces

The structures grown are illustrated in Fig. 7.13. In these five structures, the location of Mn ions are systematically changed with respect to the distance from the interface.

Structure (1) is a case where the whole interface is covered with one unit cell of $SrMnO_3$ followed by a thick layer of $SrRuO_3$. The fabrication was carried out by monitoring the recovery of the diffracted RHEED intensity. This structure can be viewed as a metal-insulator-semiconductor structure with $SrMnO_3$ as the insulator since $SrMnO_3$ is reported to be a G-type antiferromagnetic insulator [21, 22] with a calculated band gap of 0.3 eV [23]. The semiconducting behavior can also be confirmed from the resistivity of a single film of $SrMnO_3$ deposited on $SrTiO_3$ (001) shown in Fig 7.14(a). Assuming a thermal activation type transport, a linear fitting in the semilogarithmic plot gives an activation energy of 0.12 eV, which is of similar

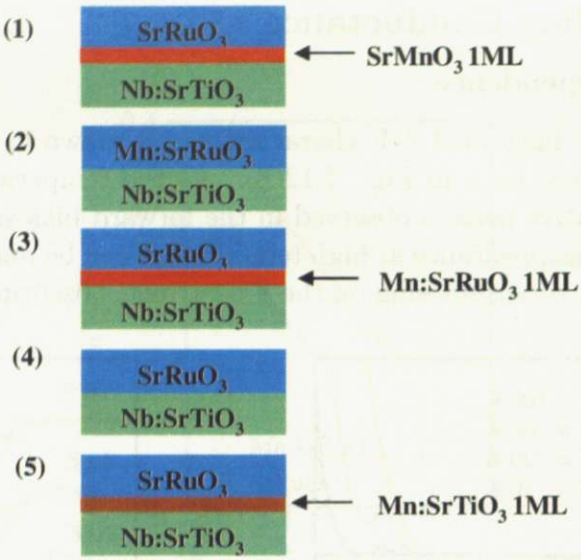


Figure 7.13: Schematic diagram of the artificial structures grown for systematic localization of Mn ions at specific distance from the interface.(1) $SrRuO_3/[SrMnO_3]_{1ML}/Nb:SrTiO_3$, (2) $Mn:SrRuO_3/Nb:SrTiO_3$, (3) $SrRuO_3/[Mn:SrRuO_3]_{1ML}/Nb:SrTiO_3$, (4) $SrRuO_3/Nb:SrTiO_3$, (5) $SrRuO_3/[Mn:SrTiO_3]_{1ML}/Nb:SrTiO_3$.

order to the calculated value. It should be remembered that transport measurement is not always a good measure of band gaps in strongly correlated insulators.

The decrease in the current and the positive shift in the onset voltage at forward bias with reduction in temperature in Fig 7.14(b) contrasts with the behavior observed for direct metal-semiconductor contact in $SrRuO_3/Nb:SrTiO_3$. This can be attributed to the presence of a thermally activated process in addition to the TFE process. We believe that the electron density in the conduction band of $SrMnO_3$ decreases with decrease in temperature, effectively increasing the tunneling barrier resulting in significant reduction in the forward and reverse bias current. It is evident from the $I$-$V$ results that no current peak was observed in this structure.

Structure (2) is the observed case where the surface of $Nb:SrTiO_3$ is covered with $Mn:SrRuO_3$. In Structure (3), a unit cell of $Mn:SrRuO_3$ is inserted between a thick layer of $SrRuO_3$ and $Nb:SrTiO_3$. In this case the basic feature of the temperature dependence of the $I$-$V$ characteristics are the same as those observed in $SrRuO_3/Nb:SrTiO_3$ but with the presence of current peaks at low temperatures resembling the results for Structure (2). This is an indication that the origin of the current peak is caused by the local structure at the interface between $Mn:SrRuO_3$ and $Nb:SrTiO_3$.

The extreme case simulating a situation where the Mn ions are embedded inside $Nb:SrTiO_3$ is demonstrated in Structure (5). Here a 5 % Mn doped $SrTiO_3$ is deposited on $Nb:SrTiO_3$ followed by a thick layer of $SrRuO_3$. There has not been any report on the band calculation of Mn-doped $SrTiO_3$, however from investigation of leakage current at metal/$Mn:SrTiO_3$ contacts, $Mn:SrTiO_3$ can be assumed to be

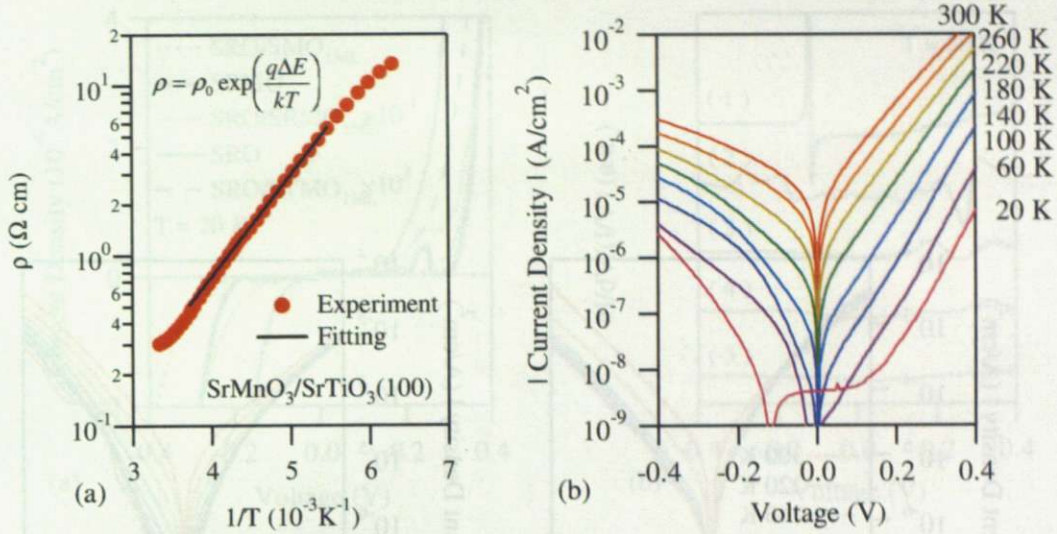


Figure 7.14: (a) Temperature dependence of the resistivity of $SrMnO_3/SrTiO_3$ (001) thin film exhibiting a semiconducting behavior. (b) The temperature dependent $I$-$V$ characteristics of Structure (1) in Fig. 7.13 demonstrating a large reduction with decrease in temperature.

insulators [24,25] although in some cases the Mn valence is reduced to $Mn^{2+}$ or $Mn^{3+}$ and forms complexes with oxygen vacancies such as $V_O^{\cdot\cdot}$-$Mn^{2+}$ [26,27]. In the present case, we assume them to be insulators with negligibly small conductivity. The $I$-$V$ characteristics for the two different insertion layers of Mn:$SrTiO_3$ are presented in Fig. 7.15(c) and (d). The temperature dependence strongly resembles that of $SrRuO_3$/Nb:$SrTiO_3$ with no sign of current peaks at low temperatures.

The above investigations reveal that the appearance of the low temperature current peaks are associated with the presence of Mn ions at the metal side in a diluted form. This rejects the possibility of Mn embedded in the substrates by diffusion or implantation during growth acting as an ionic potential inside the depletion region as has been reported in some cases [28,29].

A summary of the $I$-$V$ characteristics and the derived conductance results are shown in Fig. 7.16(a) and (b) for all the structures mentioned above. The appearance of the current peak is observable only in Structures (2) and (3).

### Growth Condition Dependence

The phenomenon of low temperature current peaks have also been observed in Mn:$SrRuO_3$/Nb:$SrTiO_3$ junctions grown under different oxygen partial pressures $P_{O2}$. The temperature dependence of the $I$-$V$ characteristics are displayed in Fig. 7.16. It is evident that under $P_{O2} = 0.3$ and 0.5 Torr current peaks appear, but not for $P_{O2} = 0.1$ or 1.0 Torr implying that $P_{O2}$ is also an important factor in the appearance of the NDR behavior.

A systematic change in the $I$-$V$ characteristics is observed with variation in the oxygen pressure. The $I$-$V$ characteristics exhibit non-symmetric behavior evolving

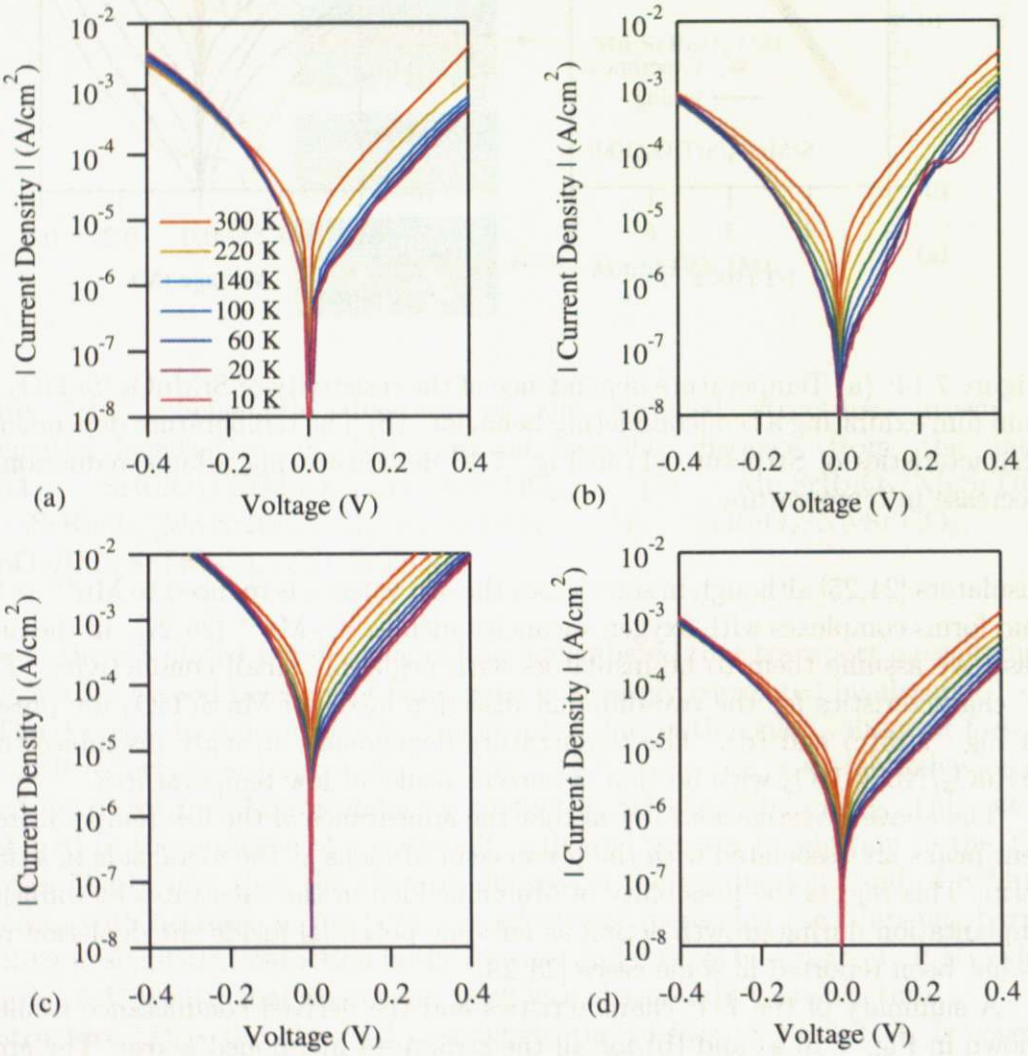


Figure 7.15: $I$-$V$ characteristics for Schottky junctions between Nb:$SrTiO_3$ and the metal side modified to (a) $SrRuO_3$/Nb:$SrTiO_3$ (Structure (4)), (b) $SrRuO_3$/[Mn:$SrRuO_3$]$_{1ML}$ (Structure (3)), (c) $SrRuO_3$/[Mn:$SrTiO_3$]$_{1ML}$ (d) $SrRuO_3$/[Mn:$SrTiO_3$]$_{3ML}$ (Structure 5).

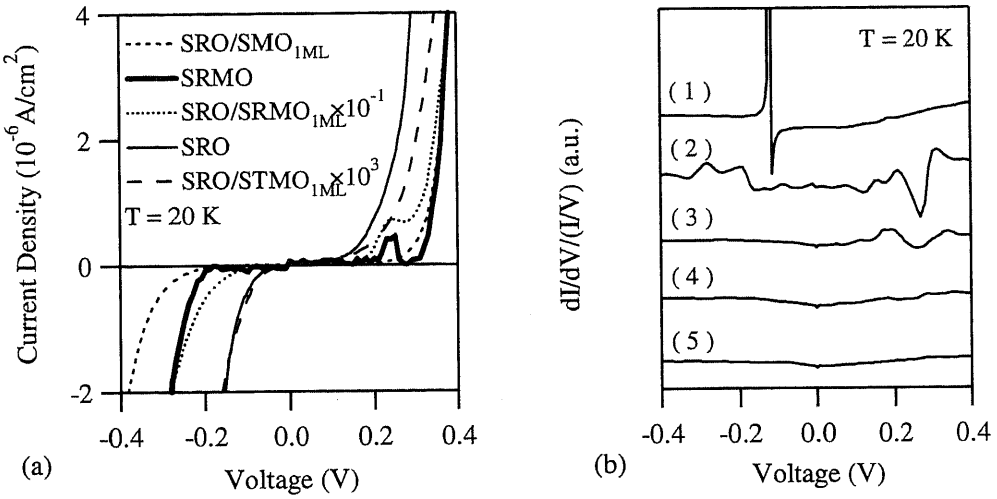


Figure 7.16: $I$-$V$ characteristics and the conductance of the modified metal structures in Fig. 7.13. Negative peaks observed in Structures (2) and (3) in (b) corresponds to the current peaks in (a). The large spike in Structure (1) corresponds to an artifact of the non-zero crossing on the voltage axis.

to symmetric $I$-$V$ characteristics as the oxygen pressure is increased. In addition, the plateau in the small biased region is reduced as the oxygen pressure is increased. At $P_{O2} = 1.0$ Torr, almost no rectification is observed. It should be mentioned that a current peak was never observed in any of the $SrRuO_3$/Nb:$SrTiO_3$ junctions grown at different $P_{O2}$.

The systematic change in the $I$-$V$ characteristics can be compared with the systematic change in the lattice constants of the thin films grown under different oxygen pressures shown in Fig. 7.18. The increase in oxygen pressure leads to closer lattice constant of the bulk $c$-axis lattice constant.

### 7.5.3 Electron Energy Loss Spectroscopy

In order to confirm the presence of Mn ions at the interface of Mn:$SrRuO_3$/Nb:$SrTiO_3$, electron energy loss spectroscopy was taken with the aim of studying the valence of the Mn cations at the interface. A superlattice structure $SrRuO_3$/$SrTiO_3$ /15%-Mn:$SrRuO_3$/$SrTiO_3$/5%-Mn:$SrRuO_3$/$SrTiO_3$(001) was fabricated as shown in Fig. 7.19(a). From the scanning transmission electron microscopy image in Fig. 7.19(b), the atomically abrupt interface can be observed between the substrate and the first layer of the Mn:$SrRuO_3$, which assures us that the Schottky junctions measured have also abrupt interfaces with low density of defects or interdiffusion. From the EELS spectra in Fig. 7.19(c), it is evident that Mn ions are only present in the Mn:$SrRuO_3$ layers but not in the $SrRuO_3$ layers. On the assumption that Mn is substituting the Ru site in Mn:$SrRuO_3$, it is natural to think that the valence of Mn to be in $Mn^{4+}$ state, however there are reports claiming the existence of $Mn^{3+}$ [30]. In these cases, it is proposed that a charge dispropornation is taking place in the

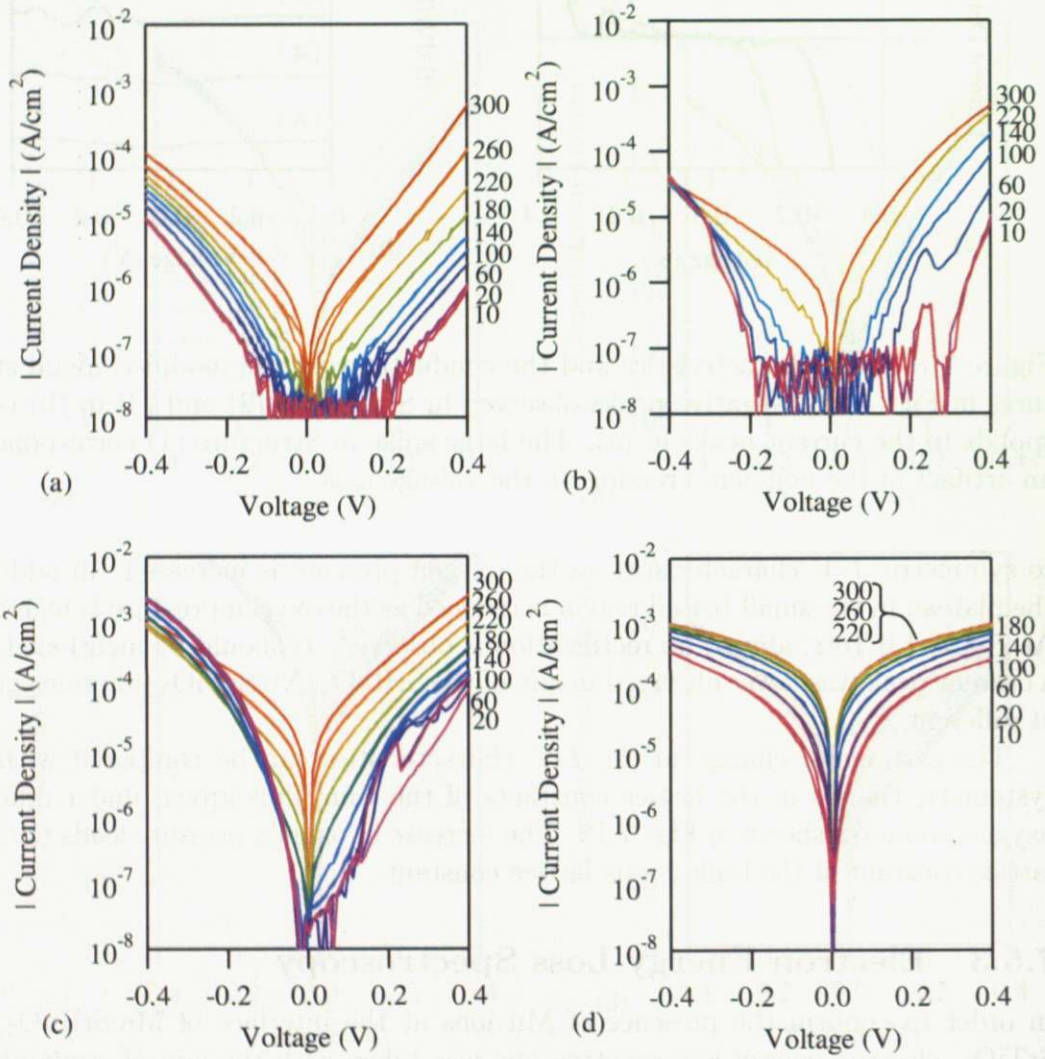


Figure 7.17: Temperature dependent $I$-$V$ characteristics for Mn:$SrRuO_3$/Nb:$SrTiO_3$ junctions grown at oxygen partial pressure of (a) 0.1 Torr, (b) 0.3 Torr, (c) 0.5 Torr and (d) 1.0 Torr. The systematic change in can be observed with current peaks appearing only in junctions grown under limited range of oxygen pressure.

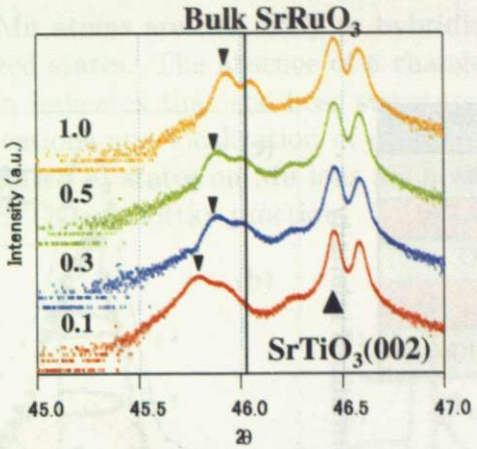


Figure 7.18: X-ray diffraction pattern of $Mn:SrRuO_3/Nb:SrTiO_3$ around $Nb:SrTiO_3(002)$ peak fabricated under different partial oxygen pressures.

form, $Mn^{4+} + Ru^{4+} \rightleftharpoons Mn^{3+} + Ru^{5+}$. From the EELS spectra in Fig. 7.19(c), the valence of the Mn inside $Mn:SrRuO_3$ is likely to be between $Mn^{3+}$ and $Mn^{4+}$ by referring to the spectra obtained in oxides with different manganese valence states (Fig. 7.20 [31]).

### 7.5.4 Discussions

The tunneling current density is a function of the transmission probability, and the occupancy in the initial and the final states. Effect on any of the three parameters would give rise to a change in the tunneling current. In the present case, the NDR behavior resembles a typical resonant tunneling diode in which some localized state is acting as the well. Possible origin of the localized state can be inferred by considering the electronic structure of $Mn:SrRuO_3$.

There has not been any theoretical or experimental study of the electronic structure in $Mn:SrRuO_3$. Therefore we base our discussion on the electronic structure deduced from the two extreme compounds $SrRuO_3$ and $SrMnO_3$. From optical spectroscopy of $SrRuO_3$, it is reported that the crystal field splitting $10Dq$ and the charge transfer gap $\Delta_{pd}$ are both $\sim 3$ eV [32]. In $SrRuO_3$, the oxygen $2p$ band lies below the $t_{2g}$ band and the Fermi level is located inside the $t_{2g}$ band as shown in Fig. 7.21(a). The electronic structure of $SrMnO_3$ is more complicated due to the existence of hexagonal and cubic structures as well as the stable phase formation of $SrMnO_{3-\delta}$ [33]. Here we base our discussion on $SrMnO_3$ with a cubic G-type antiferromagnetic ground state. From theoretical calculation, an energy band diagram can be drawn as shown in Fig. 7.21(a). Here the top of the valence band overlaps with the oxygen $2p$ band and the Mn $e_g$ bands are located $\sim 0.6$ eV above the Fermi level [23]. When Mn is substituted for Ru in $Mn:SrRuO_3$, within a rigid band picture, the band structure is expected to be similar to that of $SrRuO_3$ but with a slight modification in the empty states arising from the Mn $3d$-$e_g$. Owing to the smaller spatial distribution of $3d$ orbitals in Mn compared with that of $4d$

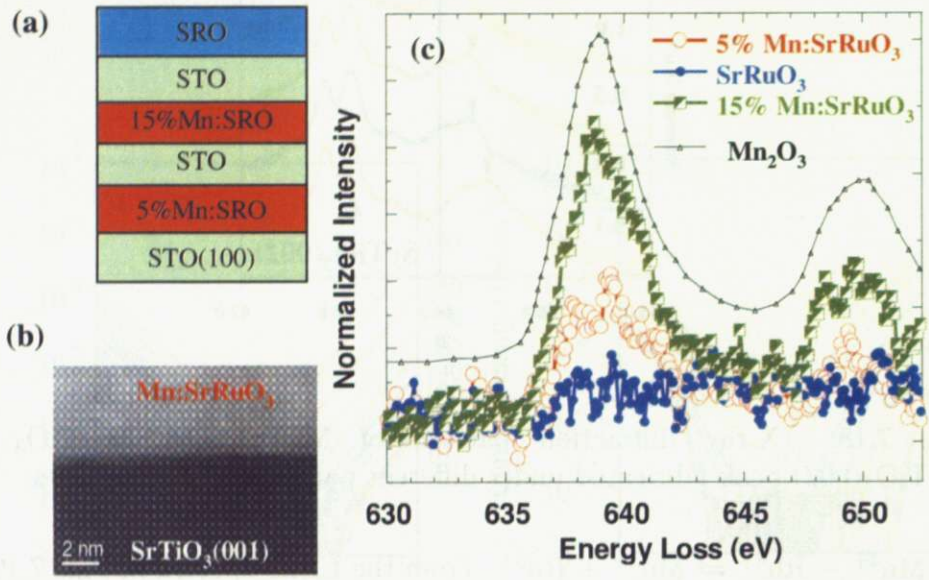


Figure 7.19: (a) Schematic diagram of the $Mn:SrRuO_3/SrTiO_3$ superlattice structure, (b) the STEM image of the substrate-thin film interface, and (c) the electron energy loss spectroscopy spectra of the superlattice.

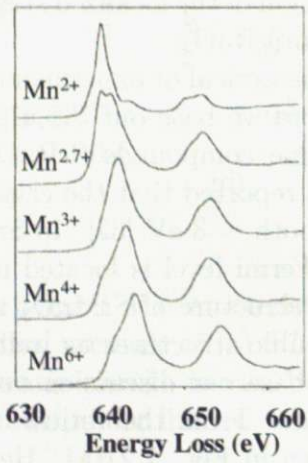


Figure 7.20: EELS spectra for Mn-oxides of various valence states [31].

in Ru, the $e_g$ state on Mn atoms are less likely to hybridize with the surrounding oxygen and form localized states. The absence of a change in the lattice constant by 5 % Mn substitution indicates that the host structure is retained even under substitution of smaller cations and localization of $e_g$ state is further stressed. We can expect that the localized $e_g$ states on Mn ions are acting as the resonant state in the Mn:$SrRuO_3$/Nb:$SrTiO_3$ Schottky junction.

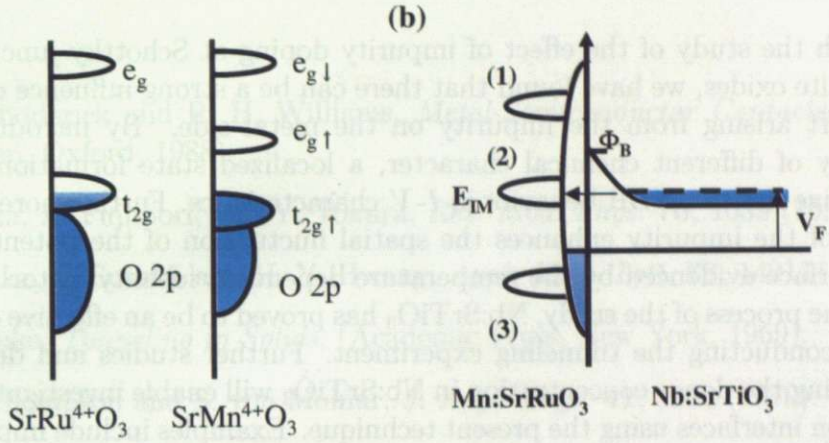


Figure 7.21: (a) Schematic density of states for $SrRuO_3$ and $SrMnO_3$. (b) Band diagram illustrating the localized Mn $e_g$ state at various energy levels relative to the Schottky barrier heights: (1) $E_{IM} > \Phi_{SB}$, (2)$E_F < E_{IM} < \Phi_{SB}$, (3) $E_{IM} < E_F$. Only in case (2), can the resonant tunneling behavior can be seen.

We have also shown that the NDR behavior is not always observed, but only in junctions grown under certain oxygen pressure $P_{O2}$. The systematic change in the lattice constant with $P_{O2}$ indicates that the oxygen pressure is influencing the degree of distortion in the host lattice. The change in the lattice constant will change the relative energy level of the Mn $e_g$ level which is related to the appearance of the NDR behavior as explained below.

If the localized state is located at an energy level above the SBH, then no NDR behavior would appear in the *I-V* characteristics because the drift current will be dominating when such a large forward bias is applied. This is the situation depicted as (1) in Fig. 7.21(b). When the localized state is lower than the barrier height but above the Fermi level, the tunneling current is expected to be modified by the change in the final state of the localized state at small forward bias which is the situation depicted as (2) in Fig. 7.21(b). Finally, we can imagine a situation where the localized state is located below the Fermi level, corresponding to case (3) in Fig. 7.21(c), in which case the localized state is filled, hence no characteristic feature can be expected under forward bias. A difference in the reverse bias may arise because of the modified initial states but it is expected to be smeared out by the large density of states of the host. The junctions in which NDR behavior appear are in the regime where the localized state is located in between the Fermi level of $SrRuO_3$ and the Schottky barrier height. Indeed, from our previous investigation, the Schottky barrier height in this system is 1.47 eV which is much higher than the

observed peak voltages at forward bias.

In summary, the appearance of the NDR behavior is strongly related to the relative energy level of the localized state which is strongly modified by the lattice distortion of the host.

## 7.6 Conclusions

Through the study of the effect of impurity doping at Schottky junctions between perovskite oxides, we have found that there can be a strong influence on the current transport arising from the impurity on the metal side. By introducing a metal impurity of different chemical character, a localized state formation is evidenced which give rise to a NDR behavior in $I$-$V$ characteristics. Furthermore, the localized nature of the impurity enhances the spatial fluctuation of the potential barrier at the interface evidenced by the temperature dependent ideality factor.

In the process of the study, Nb:$SrTiO_3$ has proved to be an effective electron emitter for conducting the tunneling experiment. Further studies and development in controlling the donor concentration in Nb:$SrTiO_3$ will enable investigation of various effects on interfaces using the present technique. Examples include impurity induced Mott transition or magnetic impurities in a non-magnetic metallic perovskite oxide host.

# Bibliography


[1] E. H. Rhoderick and R. H. Williams, *Metal-Semiconductor Contacts*, 2nd ed. (Clarendon, Oxford, 1988).

[2] M. Imada, A. Fujimori, and Y. Tokura, *Rev. Mod. Phys.* **70**, 1039 (1998).

[3] Y. Kozuka, T. Susaki, and H. Y. Hwang, *Appl. Phys. Lett.* **88**, 142111 (2006).

[4] C. B. Duke, *Tunneling in Solids*, (Academic Press, New York, 1969).

[5] W. A. Thompson and S. von Molnar, *J. Appl. Phys.* **41**, 5218 (1970).

[6] H. Suzuki, M. Iyori, T. Yamamoto, S. Suzuki, K. Takahashi, T. Usuki,and Y. Yoshisato, *Jpn. J. Appl. Phys.* **31**, 2716 (1992).

[7] F. Fukunaga and N. Tsuda, *J. Phys. Soc. Japan* **63**, 3798 (1994).

[8] G. Cao, S.McCall, J. Bolvier, M. Shepard, F. Freibert, P. Henning, and J. E. Crow, *Phys. Rev. B* **54**, 15144 (1996).

[9] L. Pi, A. Maignan, R. Retoux, and B. Raveau, *J. Phys: Condens. Matter* **14**, 7391 (2002).

[10] C. Bansal, H. Kawanaka, R. Takahashi, and Y. Nishihara, *J. Alloys. Comp.* **360**, 47 (2003).

[11] G. N. Banerjee, R. N. Bhowmik, and R. Ranganathan, *J. Phys: Condens. Matter* **13**, 9481 (2001).

[12] G. Cao, S. Chikara, X. N. Lin, E. Elhami, V. Durairaj, and P. Schlottmann, *Phys. Rev. B* **71**, 035104 (2005).

[13] T. Sugiyama and N. Tsuda, *J. Phys. Soc. Japan* **68**, 1306 (1999).

[14] R. Mathieu, A. Asamitsu, and Y. Kaneko, J. P. He, X. Z. Yu, R. Kumai, Y. Onose, N. Takeshita, T. Arima, H. Takagi, and Y. Tokura, *Phys. Rev. B* **72**, 092404 (2005).

[15] T. Yamamoto, S. Suzuki, K. Kawaguchi, and K. Takahashi, *Jpn. J. Appl. Phys.* **37**, 4737 (1998).

[16] M. Hiratani, C. Okazaki, K. Imagawa, and K. Takagi, *Jpn. J. Appl. Phys.* **35**, 6212 (1996).

[17] H. Y. Lee, H.-M. Christen, M. F. Chisholm, C. M. Rouleau, and D. H. Lowndes, *Appl. Phys. Lett.* **84**, 4107 (2004).

[18] J. H. Werner and H. H. Guttler, *J. Appl. Phys.* **69**, 1522 (1990).

[19] H. Hasegawa and T. Nishino, *J. Appl. Phys.* **69**, 1501 (1991).

[20] R. Tsu and L. Esaki, *Appl. Phys. Lett.* **22**, 562 (1973).

[21] T. Takeda and S. Ohara, *J. Phys. Soc. Jpn.* **37**, 275 (1974).

[22] K. Kikuchi, H. Chiba, M. Kikuchi, and Y. Syono, *J. Solid State Chem.* **146**, 1 (1999).

[23] R. Soendena, P. Ravindran, S. Stoelen, T. Grande, and M. Hanfland, *Phys. Rev. B* **74**, 144102 (2006).

[24] W. Hofman, S. Hoffmann, and R. Waser, *Thin Solid Films* **305**, 66 (1997).

[25] K. Morito, T. Suzuki, and M. Fujimoto, *Jpn. J. Appl. Phys.* **40**, 5493 (2001)

[26] R. A. Serway, W. Berlinger, K. A. Muller, and R. W. Collins, *Phys. Rev. B* **16**, 4761 (1977).

[27] V. V. Lemanov, E. P. Smirnova, A. V. Sotnikov, and M. Weihnacht, *Phys. Solid State* **46**, 1442 (2004).

[28] S. Modesti, D. Furlanetto, M. Piccin, S. Rubini, and A. Franciosi, *Appl. Phys. Lett.* **82**, 1932 (2003).

[29] G. D. J. Smit, S. Rogge J. Caro, and T. M. Klapwijk, *Phys. Rev. B* **69**, 125324 (2004).

[30] R. K. Sahu, Z. Hu, M. L. Rao, S. S. Manoharan, T. Schmidt, B. Richter, M. Knupfer, M. Golden, J. Fink, and C. M. Schneider, *Phys. Rev. B* **66**, 144415 (2002).

[31] H. Kurata and C. Colliex, *Phys. Rev. B* **48**, 2102 (1993).

[32] Y. S. Lee, J. S. Lee, T. W. Noh, D. Y. Byun, K. S. Yoo, K. Yamaura, and E. Takayama-Muromachi, *Phys. Rev. B* **67**, 113101 (2003).

[33] K. J. Lee and E. Iguchi, *J. Solid State Chem.* **114**, 242 (1995).

# Chapter 8

# Conclusions

The attractive physical properties of transition metal oxides have motivated researchers to design devices which would bring a paradigm shift to the world of electronic devices. In order to navigate ourselves towards the era of oxide electronics, we should remind ourselves of the achievements on which the present semiconductor technology is established. These are (1) improvement in the quality of the materials, (2) the development of interface physical concepts, and (3) the development of new characterization techniques. All can be said to be universal criteria for device research and development in any materials system.

The present oxide electronics is positioned at an adolescence stage where the underlying physics of many phenomena are beginning to be unveiled and the basic fabrication methodologies established. To shift the research level to the next phase, now or never is the time to make progress in the field of interface physics and development of suitable characterization techniques. This research began with a motivation to be a leading example of such an attempt.

Schottky junction was selected as the model interface in this study which contains the three essential interface concepts to explore the characteristic features found in oxides. Compared with field effect structures and heterojunctions, Schottky junctions have the advantage of been simple still exhaustive in containing the essential concepts of interface physics. For conducting the study, a characterization technique suitable for oxide interface has been designed, modified and installed. Application of internal photoemission technique in characterizing Schottky junctions has played the important role as an independent measure of the SBH at thermal equilibrium unlike the $I$-$V$ or $C$-$V$ methods, which require application of bias voltage. Although simple in principle and widely known in conventional semiconductors, internal photoemission has never been performed in oxide interfaces up to now, which shows that we are still at the very early stages in the field. To further accelerate the study of oxide interfaces, two effective applications of this technique can be proposed.

First is the addition of a dc voltage source. A dc voltage supply in series with the interface of interest will enable conductivity measurements between semiconductor-insulator and even insulator-insulator heterojunctions, which is difficult because of the difficulty in forming Ohmic contacts to insulators. Typical examples include band offset measurements at interfaces between two insulators with different polarities as in $SrTiO_3/LaAlO_3$, or doping carriers into Mott insulators such as $La_2CuO_4$,

in which carrier injection is expected to change the conductivity drastically.

Second is the measurement of hot electron mean free path in metals. The mean free path of electrons a few eV above the Fermi level inside a metal can be as long as 100 nm. In vacuum photoemission, the electron mean free path in this energy range cannot be measured because the energies are below the work function of the metals. By measuring IPE spectra of Schottky junctions with different thickness of metal overlayers, the electron mean free path can be obtained in energy region few eV above the Fermi level. This is important in designing hot electron transistors as has been demonstrated in magnetic materials as well as in normal semiconductors. For example, by using the magnetic field sensitive $La_{0.7}Sr_{0.3}MnO_{3-\delta}$ as the base in a transistor, the electron transmission efficiency from the emitter to the collector can be tuned by magnetic field.

It can be said that, now is the time and perovskite oxides are the materials in which we can appreciate the full strength of the IPE technique.

An overview of the strategy taken in the study of perovskite specific features on the interface electronic structure is summarized in Fig. 8.1. The phenomenological evidence have been discussed based on the application of conventional theories (process 1), before introducing the on-going theories of the perovskite physical properties (processes 2 and 3).

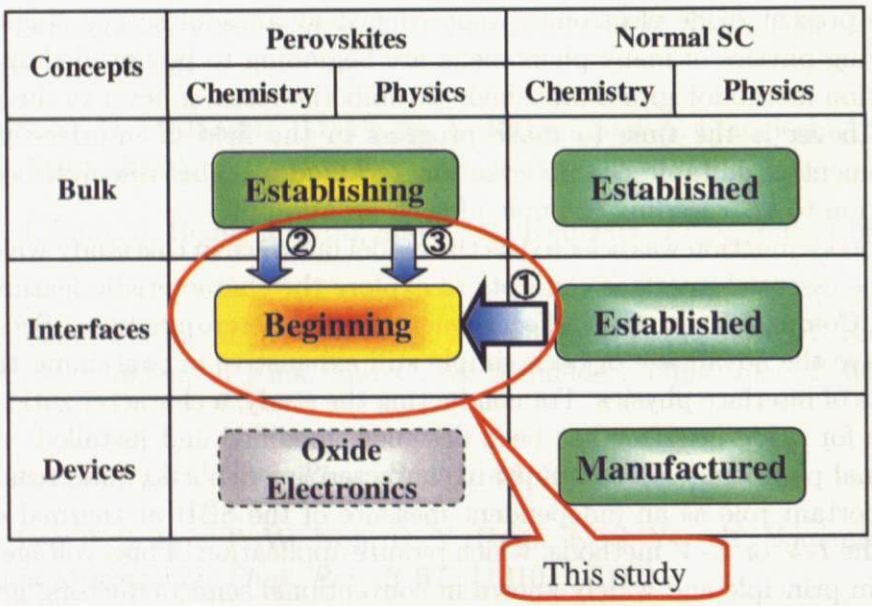


Figure 8.1: The roadmap to oxide electronics and the relative stage of this study. The perovskite interface concepts have been discussed by application of (1) conventional interface concepts, perovskite bulk (2) chemical properties, and (3) physical properties.

Through studies of perovskite Schottky junctions, the conventional concepts of interface physics can be said to be applicable in general at the fundamental level.

However, for detailed understanding, the perovskite specific features demands modifications in certain cases. For example, the electric field dependence in the bulk dielectric permittivity in incipient ferroelectric semiconductors strongly modifies the band bending. This feature is important considering the dominance of $SrTiO_3$ as the prototype semiconductor in this system, and the relatively high range of doping concentration that can be achieved. The latter fact limits the use of $SrTiO_3$ in the degenerate regime and not in the non-degenerate regime. In the degenerate regime, the reduction of the depletion width from the electric field dependent permittivity favorably enhances the speed of the device operation.

The classical concepts of SBH formation have proved to be applicable to perovskite system to a satisfactory level with additional insights. We have confirmed cases in which the Schottky-Mott relation is valid, namely the $SrRuO_3$/Nb:$SrTiO_3$ junctions, and cases where interface states or in-gap states are likely playing an important role, as in the manganite/Nb:$SrTiO_3$ cases. In the latter case, these states posses the character of the manganite suggesting the importance of local electronic structure on the metal side, in contrast to the classical Schottky junctions where screening length in the metal is negligible. What is phenomenologically observed as *interface states* may actually be intrinsic properties of the perovskites, as is suggested from one of the origins for the magnetic field dependent SBH in manganite junctions. The existence of systems in which the SBH is explicable by simple bulk properties and systems requiring local chemistry is reminiscent of the conventional Schottky junctions. However, the significant difference in the perovskite systems is that the origin of the SBH formation mechanism needs to be considered not only from the semiconductor surface states but also from the surface electronic structure of the metals. This is because of the sensitivity to structural distortion by variance in composition, defects, or strain, on the electronic energy levels of the $BO_6$octahedtra altering the spatial orientation of the chemical bonds, hence the SBH. Therefore, the effect of interface local chemical bonds on the formation of SBH is more important in the perovskite than in the conventional interfaces.

The importance of the local chemical bonds at the interfaces can also be evidenced in the nature of interface states in perovskite junctions. The resonant tunneling behavior and the increasing potential fluctuation at the interface originate from the relatively long screening length of impurities. These findings suggest possibilities to design resonant states based on characteristic overlaps of impurity wave functions with the host, rather than by tuning the energy band offsets between different materials. This is a completely new concept for designing resonant diodes determined not by the lattice mismatch but from the characteristic screening length of the impurities.

For further development in the studies of perovskite interfaces, the classical description of interfaces based on the *band* picture may not be suitable and a description in terms of *bonds* may be a better starting point. The sensitivity to microscopic effects is due to the compositional and structural complexity of the constituents and the associated electronic and the lattice degrees of freedom. The former part is strongly related to the chemistry of oxides in which the celebrated high quality of thin films may need to be improved to a higher level for interface studies, due to the sensitivity of the physical properties of perovskites to non-stoichiometry, such as

cation off stoichiometry and oxygen vacancies. This is a challenging task considering the numerous hidden parameters involved in PLD method, the lack of effective technique for characterization of off-stoichiometry with efficiency and ease, and the small volume of the materials involved. The latter part is the physical property inherent to oxides. The interface properties influenced by subtle change in the environments stem from the less itinerant and spatially oriented nature of the $d$-orbitals. Derived properties include, crystal field splitting, non-bonding orbitals having spin degree of freedom, narrow density of states, etc.

Although we have seen many aspects of these features in this study, we have not addressed the issue of electron-electron interaction effect on interface parameters. We believe that understanding of heterointerfaces between doped Mott insulators would be the next important step in establishing the framework of perovskite interface physics. The scientific importance lies in the question, how do we incorporate the many body effect in the theory founded on single particle physics? Depletion, band gaps, band offsets, etc are expected to require strong modification if we base our discussion on the bulk properties of perovskites. Simultaneously, the redistribution of charges necessarily taking place at the interface may obscure the many-body effect resulting in an interface specific phase formation, similar to the case of silicide formation at metal/Si interfaces but driven by charge redistribution rather than chemical reactions. We believe that the first challenge in the study of interfaces between Mott systems would be to conduct an experiment in which the electron correlation effect can be isolated from other effects.

We state three messages as perspectives toward future research in oxide interfaces to close this thesis. First is the importance of stoichiometry and structural perfection of the interfaces. Before discussing the physical properties of the interface in detail, it is important to clarify to what extent the interface under study is ideal. The importance should be emphasized more than in the covalent semiconductor systems because of the sensitivity of the materials to subtle changes in the chemical and physical environments. Secondly, based on the quality of the interface, we should consider the interface electronic structure both from the macroscopic band structure perspective and the microscopic chemical bonding pictures. The interesting physics is likely to be hidden in a localized region very close to the interface. Finally, in order to trigger a breakthrough in electronic devices, we should always make effort to invent devices operating on principles exclusive to perovskite interfaces. This can be imaged in analogy to the invention of a bipolar transistor from the discovery of rectification.

# Publications and Presentations

## Publications

1. Y. Hikita, Y. Kozuka, T. Susaki, H. Takagi, and H. Y. Hwang, "Characterization of the Schottky barrier in $SrRuO_3$/Nb:$SrTiO_3$ junctions," *Appl. Phys. Lett.* **90**, 143507 (2007).

2. Y. Kozuka, Y. Hikita, T. Susaki, and H. Y. Hwang, "Optically tuned dimensionality crossover in photocarrier-doped $SrTiO_3$: onset of weak localization," submitted to *Phys. Rev. B.*

3. Y. Hikita, S. Nishiki, N. Nakagawa, T. Susaki, H. Takagi, and H. Y. Hwang, "Magnetic Field Dependence of the Schottky Barrier Height at Manganite /Titanate Heterointerfaces," in preparation.

4. Y. Hikita, L. Fitting, T. Susaki, D. Muller, H. Takagi, and H. Y. Hwang, "Resonant States from Mn Impurity Doping in $SrRuO_3$/Nb:$SrTiO_3$(100) Junctions," in preparation.

## Conferences (1-3: International, 4-6: Domestic)

1. Y. Hikita, T. Susaki, H. Takagi, and H. Y. Hwang, The $12^{th}$ International Workshop on Oxide Electronics, Cape Cod MA, USA, (October 2005).

2. Y. Hikita, S. Nishiki, N. Nakagawa, T. Susaki, H. Takagi, and H. Y. Hwang, International Conference on Magnetism, Kyoto, Japan (August 2006).

3. Y. Hikita, S. Nishiki, N. Nakagawa, T. Susaki, H. Takagi, H. Y. Hwang, Materials Research Society Spring Meeting, San Francisco CA, USA (March 2007).

4. Y. Hikita, T. Susaki, H. Takagi, and H. Y. Hwang, The $66^{th}$ Japan Society of Applied Physics Autumn Meeting, Tokushima University (August 2006).

5. Y. Hikita, S. Nishiki, N. Nakagawa, T. Susaki, H. Takagi, and H. Y. Hwang, The $67^{th}$ Japan Society of Applied Physics Autumn Meeting, Ritsumeikan University (August 2006).

6. Y. Hikita, Y. Kozuka, T. Susaki, H. Takagi, and H. Y. Hwang, The $54^{th}$ Japan Society of Applied Physics Spring Meeting, Aoyama Gakuin University, (March 2007).

# Acknowledgements

This Research has been carried out under the supervision of Prof. H. Takagi and Prof. H. Y. Hwang. I would like to acknowledge both professors for giving me such a precious opportunity to experience and investigate an exciting research topic. I am especially grateful for Prof. Hwang for keeping close supervision in my activities and being kind as to share his scientific knowledge as much as the equipments and the assistance from his group members. I would like to thank Prof. M. Nohara, Dr. Y. Nakamura, and Prof. T. Sasagawa for supporting my activities outside of Takagi lab as well as the stimulating scientific discussions.

I would like acknowledge Prof. T. Susaki, a former research associate of Hwang laboratory, for supporting my practical research activities in Hwang lab and for the stimulating scientific discussions for making progress in my research to a higher level. I would like to thank Dr. N. Nakagawa and Dr. J. H. Song for fabricating the $La_{0.7}Sr_{0.3}MnO_{3(-\delta)}$ junctions to carry out the junction measurements and Mr. S. Nishiki for supporting me in the construction and initial measurements of the IPE system and for the collaboration on the $La_{0.7}Sr_{0.3}MnO_{3(-\delta)}$ junction measurements. For the scanning transmission electron microscopy and the electron energy loss spectroscopy, I would like to thank Mrs. L. Fitting Kourkoutis and Prof. D. Muller for their kind support. I would like to thank Mr. Saito for machining the sample holder.

The valuable discussions with Mr. Y. Kozuka, Dr. Y. Hotta, Dr. K. Takahashi, Dr. S. Tsuda, Mr. L. van Rees, and Dr. C. Bell have been invaluable in completing my thesis. For supporting experimental activities, I would like to thank Mr. Y. Mukunoki, Mr. G. J. W. Hassink and Mr. M. Nakayama for sharing the PLD chamber and carrying out the regular maintenance together. I appreciate the stimulating discussions and comments from the groups outside, Prof. A. Fujimori, Prof. M. Kawasaki, Dr. T. Ohnishi, Mr. K. Fujiwara, Dr. H. Nakamura, Dr. T. Takayama, and Dr. Y. Okamoto. I would like to thank the thesis committee professors, Prof. M. Oshima, Prof. Z. Hiroi, Prof. J. Yoshinobu, Prof. M. Lippmaa, and Prof. S. Nakatsuji for their scientific comments.

I would like to acknowledge the financial support from the 21st century COE for my employment as a research assistant, and the Japan Student Services Organization for scholarship support.

The daily life in the lab could not have been so smoothly spent without the support from Ms. M. Tanaka, Ms. Y. Hanada, Ms. M. Funo and Ms. K. Yashima: thank you all for your kindness.

Last of all, I give my thanks to my parents for giving me mental support.

# Physical Properties of Transition Metal Oxide Interfaces

(遷移金属酸化物界面の物性)

June, 2007

Yasuyuki Hikita